Construction and Building Materials 374 (2023) 130920

Contents lists available at ScienceDirect

Construction and Building Materials

journal homepage: www.elsevier.com/locate/conbuildmat

Strength, microstructure, CO_2 emission and economic analyses of low concentration phosphoric acid-activated fly ash geopolymer

Min He [a], Zongbao Yang [a], Ning Li [b,*], Xiaohong Zhu [c], Bo Fu [d], Zhihua Ou [a,*]

[a] School of Civil Engineering, Hunan University of Technology, Zhuzhou 412007, China
[b] Department of Mechanical, Aerospace and Civil Engineering, University of Manchester, Manchester M13 9PL, United Kingdom
[c] Department of Civil and Environmental Engineering, The Hong Kong Polytechnic University, Hung Hom, Kowloon, Hong Kong, China
[d] Collage of Civil Engineering, North Minzu University, Yinchuan 750021, China

ARTICLE INFO

Keywords:
Fly ash
Phosphoric acid
Geopolymer
Microstructure
CO_2 emission

ABSTRACT

Phosphoric acid (PA)-activated geopolymer is a potential construction material with superior mechanical performance and high temperature resistance. However, the synthesis of phosphoric acid-activated fly ash (FA) geopolymer (PAFG) usually requires high concentrations of PA. In this study, the mechanical properties and microstructure of PAFG samples prepared with varying low PA concentrations (LPA, 1–4 M), liquid/FA ratios (0.3–0.45), and curing temperatures (25, 60, 90 °C), as well as their effects on the environment and economy, were investigated. The compressive strengths of PAFG with activation of LPA were generally low. The PAFG prepared with a L/F = 0.35 and 4 M PA solution curing at 60 °C for 6 days obtained the highest compressive strength of 13.23 MPa. The formation of geopolymer gels of Si-O-Al-O-P, Al-O-P, or Si-O-P were the primary reaction products and strength gain for PAFG samples. The increase in PA concentration and L/F ratio accelerated the FA dealumination reaction and the polymerization reaction by increasing the H^+ and P-O concentrations of solution. In comparison to low concentration NaOH-activated fly ash geopolymer and cement pastes, the CO_2 emission intensity and energy consumption intensity of PAFG curing at 25 °C were reduced by 70.9% and 35.6%, and 90.6% and 90.6%, respectively. Albeit the cost increased by 87.4% and 30.7%, respectively. Therefore, it is essential to develop inexpensive chemical processes for the preparation of PA solutions.

1. Introduction

Portland cement (PC) is the most widely used building material, but its production requires high temperatures (1300–1500 °C) and generates large quantities of carbon dioxide (CO_2) [1].During the production of 1 tonne of cement, over 0.8 tonnes of CO_2 are emitted [2]. Compared to PC, geopolymer has a lower manufacturing temperature (<100 °C) and emits less CO_2 (44–64% reduction [3]), so it is considered an environmentally friendly material [4,5]. There are two types of geopolymer: alkali-activated geopolymer and acid-activated geopolymer. Alkali-activated geopolymers are synthesized in the presence of alkaline activators (such as NaOH and sodium silicate), and their chemical structure units consist of -Si-O-Al-O-, Si-O-Al-O-Si-O-, and -Si-O-Al-O-Si-O-Si-O- units [4,6]. Acid-activated geopolymers are generated in phosphoric acid (PA) medium, and their chemical structural units are constituted of -Al-O-P-O-, -P-O-Si-O-P-O-, -P-O-Si-O-Al-O-P-O-, and -P-O-P-O- units [7,8]. Alkali-activated geopolymers have received more concern over the past few decades, whereas the development of acid-activated geopolymers is relatively slow. For acid-activated geopolymers, however, there may be issues with durability and its own acid properties in engineering applications.

Phosphoric acid (PA)-activated fly ash (FA) geopolymer (PAFG) is a potential construction material with superior mechanical performance and high temperature resistance [9]. It has a promising future in wastewater treatment [10] and the solidification of organic [11] and inorganic pollutants [12]. According to Wang et al. [13,14], the primary reaction products in phosphate-based geopolymer were an amorphous structure of $SiO_2{\cdot}Al_2O_3{\cdot}P_2O_5{\cdot}nH_2O$ and a crystalline phase, aluminum hydrogen phosphate ($AlH_3(PO_4)_2{\cdot}3H_2O$), resulted in an increased strength. Pu et al. prepared PAFG with compressive strengths ranging from 3 to 21 MPa using 6.8 mol/L PA-activated FA (at a liquid-to-solid ratio of 0.3) [9]. In contrast, Mahyar et al. [15] utilized 8.7 mol/L PA-activated FA (at a liquid-to-solid ratio of 1.0) to produce PFAG with compressive strengths ranging between 15 and 22 MPa. This suggests

* Corresponding authors.
E-mail addresses: ning.li-3@manchester.ac.uk (N. Li), ouzhihua@hut.edu.cn (Z. Ou).

https://doi.org/10.1016/j.conbuildmat.2023.130920
Received 27 January 2023; Received in revised form 24 February 2023; Accepted 1 March 2023
Available online 7 March 2023

Table 1
Chemical compositions and loss of ignition (LOI) of FA.

Oxides	SiO_2	Al_2O_3	Fe_2O_3	CaO	K_2O	TiO_2	Other	LOI
FA (wt.%)	52.51	33.32	5.13	3.66	1.17	1.05	3.16	2.8

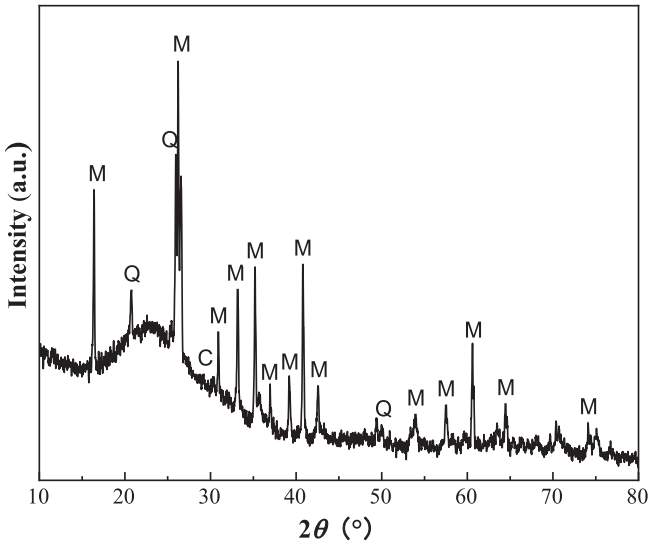

Fig. 1. XRD pattern of FA (Q-Quarts, SiO_2; M-Mullite, $3Al_2O_3{\cdot}2SiO_2$; C-Calcite, $CaCO_3$).

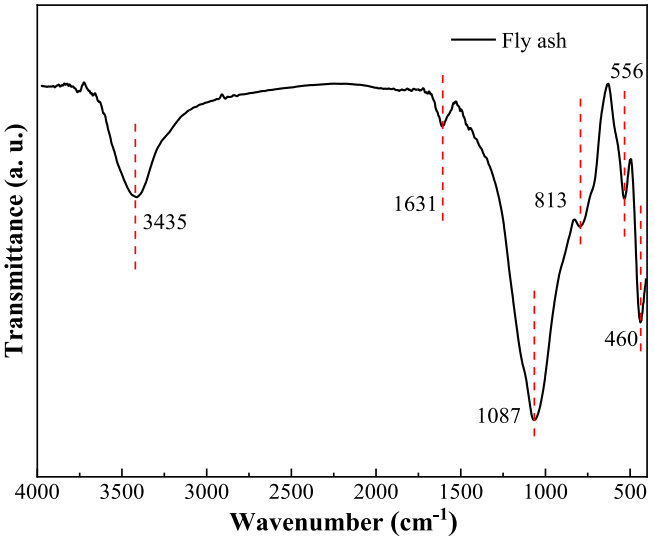

Fig. 2. FTIR spectra of FA.

that raising the concentration of PA does not necessarily improve the mechanical properties of PAFG. In addition, high concentrations of PA released considerable quantities of heat during the polymerization reaction, hence decreasing the setting of PAFG, which is detrimental to engineering applications and increases costs [16,17]. At present, there is almost no related research on PAFG synthesized using low-concentration PA (LPA).

Moreover, the research on PAFG is mainly focused on the strength and microstructures, whereas the research on the CO_2 emission and economic analyses of PAFG is also rarely involved. Previous research has demonstrated that the CO_2 emissions of alkali-activated FA geopolymer (AAFG) was 40–80% lower than that of PC concrete [18–20], while the cost was comparable or slightly higher [21–23], depending on the type and concentration of the activator used. According to the literatures [24,25], the CO_2 emission of PA was significantly lower than that of alkaline solutions [26], but the cost was much high due to the preparation process of PA involves the decomposition of phosphate rock with sulphuric acid. Therefore, it is necessary to understand the carbon emissions, energy consumption, and cost of PAFG preparation process.

In this study, low calcium FA was used as a precursor, and the effects of different LPA concentrations (LPA, 1–4 M), liquid/FA ratios (L/F, 0.3–0.45), as well as curing temperatures (25, 60, 90 °C) on the strength and microstructure of PAFG were investigated. Additionally, the carbon emissions, energy consumption, and cost of PAFG cured at various temperatures were studied and compared to AAFG and PC pastes.

2. Materials and methodology

2.1. Raw materials

To produce geopolymers, class F FA (according to the ASTM classification) from a local building materials company was used as precursor. The chemical composition of the FA was determined by X-ray fluorescence (XRF) and shown in Table 1. The FA was rich in SiO_2 and Al_2O_3 (the sum of their mass fractions greater than 80%). Fig. 1 shows the X-ray diffraction (XRD) patterns of the FA, which exhibits that FA had a certain amorphous aluminosilicate phase at between 15 and 30° 2θ. There were also some crystalline phases in FA such as quartz (Q, SiO_2), mullite (M, $3Al_2O_3{\cdot}2SiO_2$) and calcite (C, $CaCO_3$). Fig. 2 shows the FTIR spectra of FA in the range of 400–4000 cm^{-1}. The absorption peaks at about 3435 cm^{-1}, 1631 cm^{-1}, 1087 cm^{-1}, 813 cm^{-1}, 556 cm^{-1}, and 460 cm^{-1} were attributed to the bands of –OH, H-O-H, Si-O-Si (Al), Si-O-Si (Al), Si-O-Al, and Si-O bonds, respectively [27,28]. The particle size distribution was determined by laser particle size analyzer as shown in Fig. 3. The FA particle size was predominantly in the micron range, with 10% and 90% of the FA particles having a particle size no larger than 2.75 μm and 58.20 μm, respectively. The median particle size (D_{50}) of FA was 17.27 μm. The FA particles had spherical shape as shown in Fig. 4. Commercial PA solution (H_3PO_4, 85 wt%) was used to prepare a different molar concentration of activator solutions. Distilled water was used as a solvent.

2.2. Preparation

PAFG was usually prepared using 6–10 mol/L PA and a liquid-to-solid ratio of 0.3–0.5 [29,30]. To examine the effectiveness of LPA as an activator in FA geopolymer, the original PA (about 14.6 mol/L) was diluted to 1 mol/L, 2 mol/L, 3 mol/L and 4 mol/L by distilled water. The liquid-to-FA (L/F) ratios of 0.3, 0.35, 0.4 and 0.45 were used in this study, in which liquid contains original PA solution and additional water. All samples were cured at 60 °C. A relatively wide range of P/Si (0.04–0.17) and P/Al (0.05–0.23) molar ratios in system were observed and shown in Table 2. Moreover, two mix proportions with different curing temperature of 25 °C and 90 °C and a constant PA concentration of 4 mol/L and L/F ratio of 0.35 were used to investigate the influence of curing temperature. The mixture proportions of PAFG blends are presented in Table 2.

The preparation process of all paste samples was in accordance with ASTM C305 [31]. The PA solution was prepared according to the mixes in advance 24 h. Then the FA powder was added and stirred for 5 mins. The paste was cast in cylinder moulds with a diameter of 20 mm and a height of 20 mm. Then the specimens were sealed in the moulds and stored in a room at 25 ± 1 °C for 1 day. The specimens were then cured in different temperature for 6 days until mechanical testing and microstructural analyses. This curing was performed to rapidly evaluate the efficacy of LPA in the preparation of PAFG; therefore, the effect of curing time is not addressed in this study.

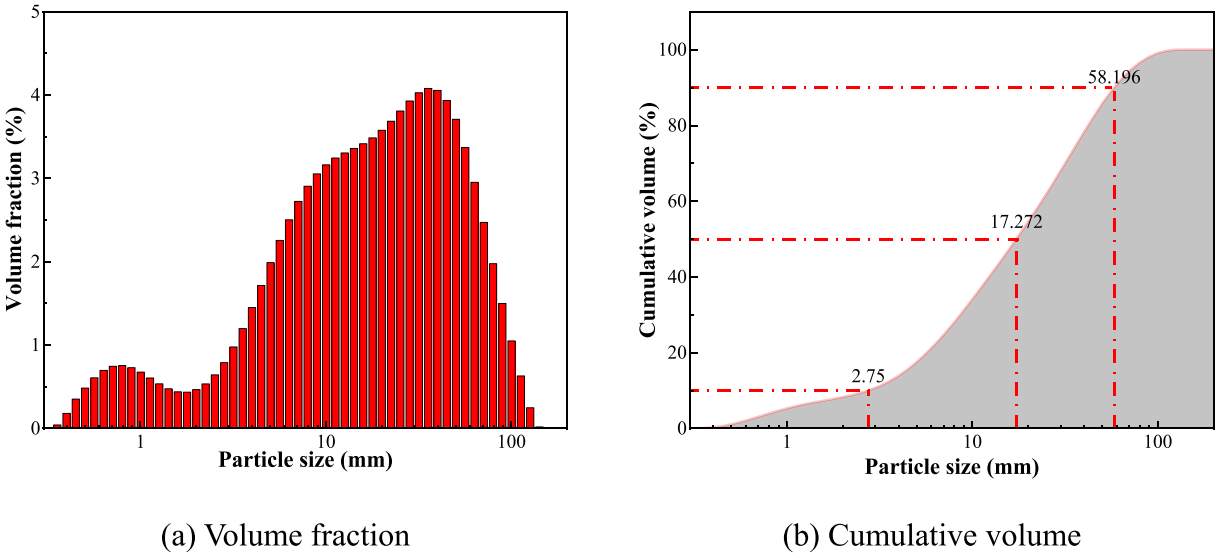

Fig. 3. Particle size distribution of FA.

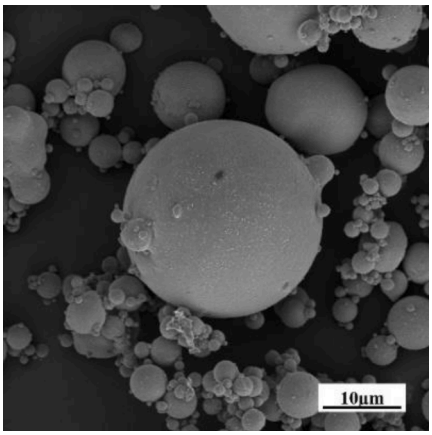

Fig. 4. SEM image of FA particles.

Table 2
Mixture proportions and chemical composition of PAFG blends.

No.	PA concentration (mol/L)	L/F ratio	Curing temperature (°C)	P/Si molar ratio	P/Al molar ratio
P1L35C60	1	0.35	60	0.04	0.05
P2L35C60	2	0.35	60	0.07	0.10
P3L35C60	3	0.35	60	0.10	0.15
P4L35C60	4	0.35	60	0.13	0.18
P4L30C60	4	0.3	60	0.11	0.15
P4L40C60	4	0.4	60	0.15	0.20
P4L45C60	4	0.45	60	0.17	0.23
P4L35C25	4	0.35	25	0.13	0.18
P4L35C90	4	0.35	90	0.13	0.18

2.3. Experimental methodology

Compressive strength was tested at 7-day by a compression machine (CSC-1101), and the average of at least three specimens was reported as result of each mix. The loading rate was 0.1 kN/s. XRD patterns of powder samples were obtained on Bruker D8 ADVANCE, using CuKα radiation. Specimens were step-scanned from 10° to 80° (2θ) at a rate of 10°/min (with step of 0.02°). Fourier transform infrared spectroscopy (FTIR) spectra were obtained on Nicolet Avatar 360 spectrophotometer. Specimens were prepared by mixing powder sample with KBr at a mass ratio of 1:200. Spectral analyses were performed over the range of 400–4000 cm^{-1} at a resolution of 2 cm^{-1}. Scanning electron microscope (SEM) was performed with Quanya-200 EDAX. The dried samples were coated with gold in advance.

3. Results and discussion

3.1. Compressive strength

Fig. 5 depicts the compressive strength of PAFG. The compressive strengths of PAFG with activation of low concentration PA were generally low, as shown in Fig. 5. This is due to the fact that the polymerization reaction of FA (Si + Al) required a higher alkaline or acid dose and curing temperature to achieve a high dissolution rate of Si and Al from precursor particles, which could consequently polymerize into a three-dimensional network structure as the load bearing structure [17,32]. The compressive strength of the samples increased by 24.44% when the concentration of PA solution was increased from 1 to 4 mol/L, from 0.52 to 13.23 MPa. The increase in PA concentration facilitated the dissolution of FA particles, which in turn facilitated the polymerization reaction and led to a substantial increase in compressive strength. Increasing the L/F ratio from 0.3 to 0.35 increased the strength by approximately 20.71%. With the PA concentration remaining constant at 4 mol/L, increasing the L/F ratio resulted in an increase in the PA content, which enhanced the strength. When the L/F ratio exceeded 0.35, the strength started to diminish. As described in the literature [33], the decrease in strength with increasing L/F ratio could be attributed to the increased porosity caused by water evaporation from the pores. In addition, increasing the curing temperature increased the compressive strength of the samples, but the effect was not very pronounced, increasing from 11 to 13.23 MPa. The geopolymerization reaction was accelerated by the elevated temperature, resulting in an increase in compressive strength [34]. However, under LPA, the limited phosphate hindered the increase in strength. A higher temperature (90 °C) was not conducive to the reaction because it was close to the evaporation temperature of free water, which caused rapid water loss and inhibited the subsequent reaction. The current PAFG has a range of strengths from 0.5 to 13 MPa and could be usually used in plastering or foundation reinforcement treatments. Additionally, the strength of PAFG could be increased by extending the curing time and increasing the PA concentration.

Fig. 6 depicts the failure patterns of PAFG with various PA

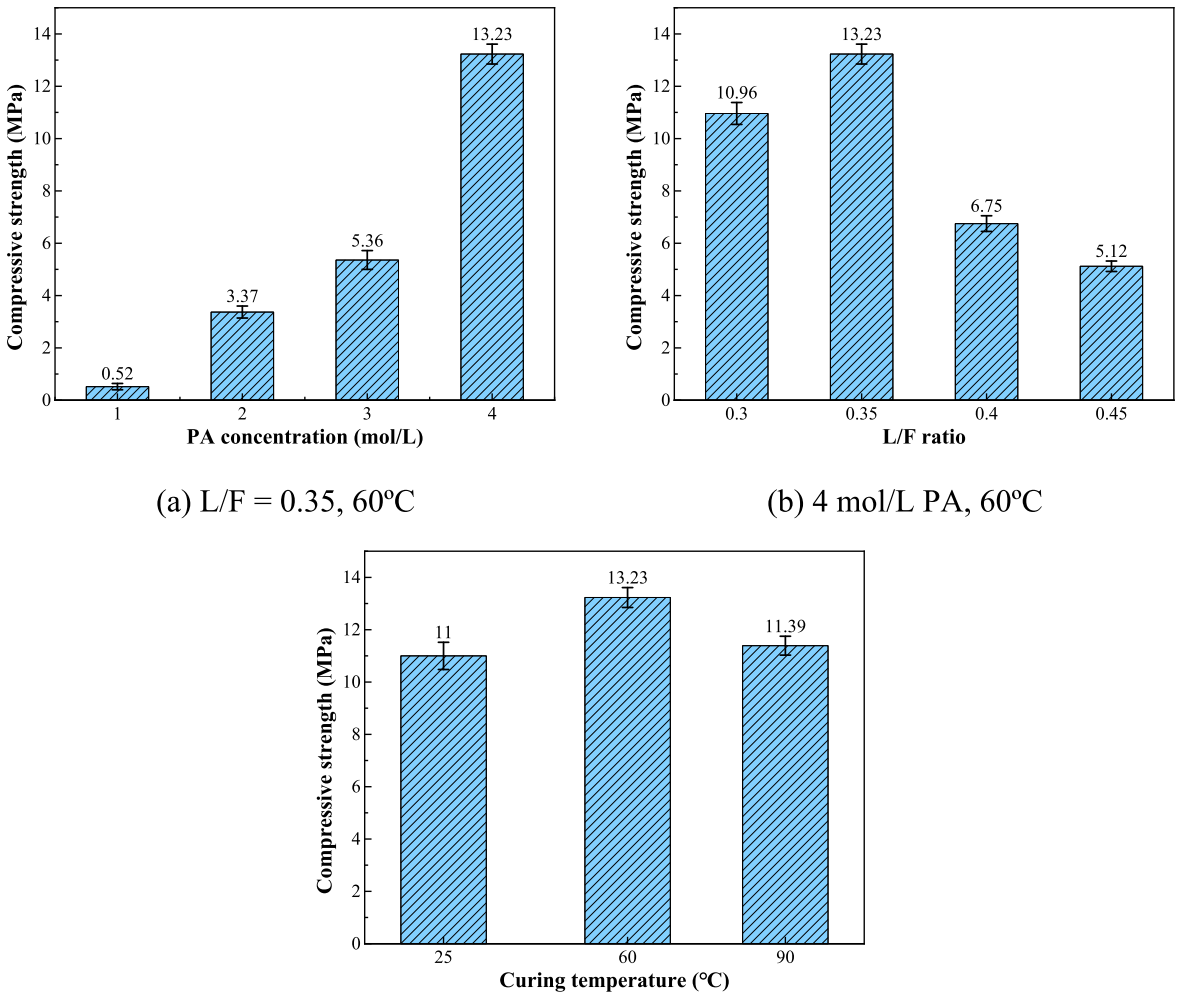

(a) L/F = 0.35, 60ºC

(b) 4 mol/L PA, 60ºC

(c) 4 mol/L PA, L/F=0.35

Fig. 5. Compressive strength of PAFG.

concentrations. The surface of the 1 mol/L PA activated PAFG sample was rough, and the damaged sample was in powder form. The failure pattern of the PAFG sample activated by 4 mol/L PA was primarily in the form of block and flake peeling, with a smooth and dense surface. This was consistent with the results of the strength test. The high PA concentration aided in the dissolution of FA particles and thus accelerated the geopolymerization reaction.

3.2. XRD analysis

Fig. 7 illustrates the XRD patterns of PAFG with varying concentrations of PA, L/F, and curing temperatures. The predominant crystal phases in PAFG were quarts (Q, SiO_2), mullite (M, $3Al_2O_3{\cdot}2SiO_2$), and calcite (C, $CaCO_3$). In comparison to the XRD pattern of FA, no new crystalline peaks appeared in PAFG samples, while C peaks faintly disappeared. Due to the LPA and the available Si and Al from FA, no P-containing crystalline phase was formed in this study. In the presence of metakaolin (rich in reactive Si and Al) and high concentration of PA, some tiny new crystalline phases were usually observed in pastes, including brushite ($CaPO_3(OH){\cdot}2H_2O$), monetite ($CaHPO_4$), and berlinite ($AlPO_4$) [9,13]. The Q and M phases were diminished, indicating that they were involved in the polymerization reaction [9,16], which was related to the PA concentration used [35]. There was a hump peak between 15 and 30° 2θ indicating the characteristic of the amorphous aluminosilicate gels of the reaction products in PAFG samples, which also contained unreacted FA in the aluminosilicate glass phase [36].

As the PA concentration and the L/F ratio increased, the crystalline peaks of Q and M shifted to more acute angles, indicating that the crystalline phases within FA were dissolved and transformed into an amorphous geopolymer gel [37,38]. The formation of geopolymer gels (Si-O-Al-O-P, Al-O-P, or Si-O-P [17]) were the primary strength gain for PAFG samples. The increase in PA concentration and L/F ratio improved the FA dealuminization reaction and accelerated the polymerization reaction by increasing the H^+ and P-O concentrations of solutions [37,38]. This increased the strength by facilitating the formation of geopolymer gels. However, an excessively high L/F ratio increased porosity of the sample, resulting in a reduction in strength.

The crystalline peaks of Q and M were slightly higher for PAFG samples cured at 25 °C and 90 °C than those cured at 60 °C. This is due to the fact that the low temperature inhibited the dissolution of FA and subsequent polymerization reaction, while the high temperature, despite facilitating the reaction, caused the system to lose water and inhibited the polymerization reaction. This demonstrates that increasing the curing temperature to 60 °C enhanced the compressive strength of the PAFG samples with activation of LPA.

3.3. FTIR analysis

Fig. 8 shows the FTIR spectrum of the PAFG sample in the range of 400–4000 cm^{-1}. The stretching vibration absorption peaks of –OH and

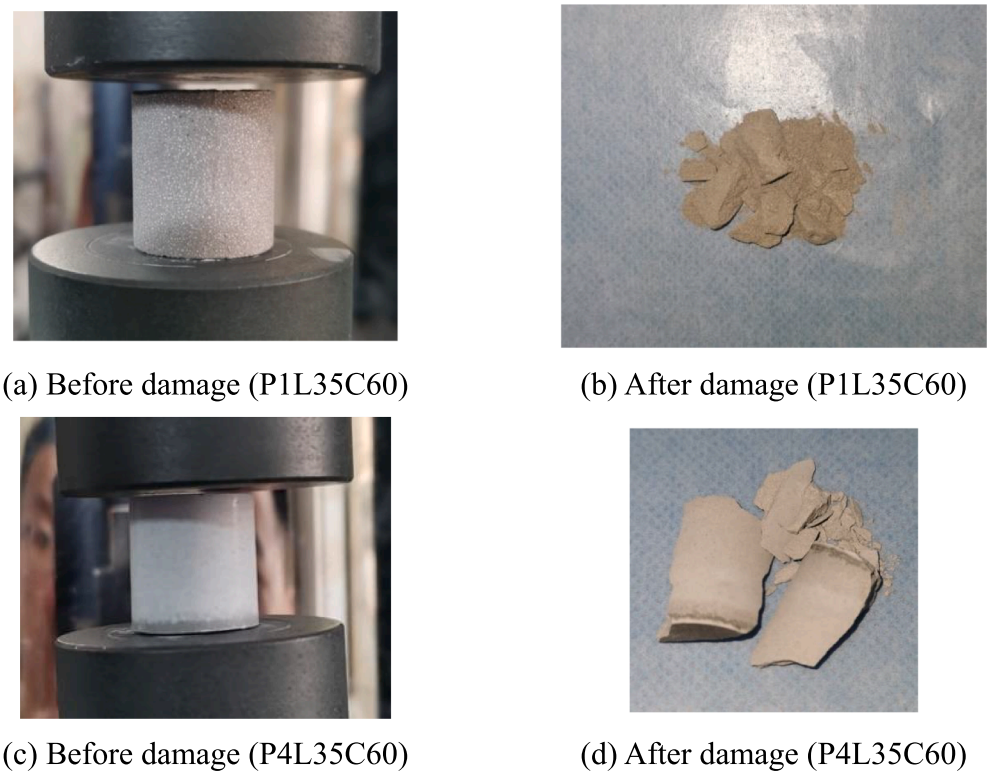

Fig. 6. Failure patterns of PAFG with different PA concentration.

H-O-H appeared at 3328–3491 cm^{-1} and 1638–1651 cm^{-1} in all the specimens, indicating the presence of chemically bound water in gels [4]. At 1074–1094 cm^{-1} the absorption peak represents stretching vibration of Si-O-Si(Al) and Si(Al)-O-P bond [35,39], which was well-known the characteristic peak results from the alkali/acid induced polymerization. The absorption peak at this range shifted to lower wavenumber region with the increase of PA concentration, indicating the interaction of P-O with silica and alumina rich gels. The bands at 809–812 cm^{-1} and 537–548 cm^{-1} were associated with the Si-O-Si(Al) band [35] and Si-O-Al [40] band in Q- and M-like structures, respectively. These peaks diminished as the polymerization reaction progressed, indicating that the P-O bond was involved in the tetrahedral network structure of Si-O-Si (Al), thereby reducing the structure's symmetry. All specimens exhibited the bending vibration band of Si-O bonds at 458–461 cm^{-1} [41]. This band has been noted in numerous previous works [9,42,43]. There was no significant change in position as the reaction conditions change, indicating that the polymerization reaction would not affect the bending of Si-O bonds.

3.4. SEM observation

Fig. 9 displays SEM images of PAFG samples with different PA concentrations. As the molar concentration of PA solution increased, the FA particles gradually dissolved, particularly the small particles within a particle size of approximately 2–5 μm. Simultaneously, the quantity of sponge-like geopolymer gel increased significantly, thereby enhancing the compressive strength of the PAFG samples.

Fig. 10 illustrates SEM images of PFAG samples with different L/F ratios. The proportion of visible unreacted FA particles decreased as the L/F ratio increased, while the proportion of geopolymer gel increased. As the value of L/F was increased to 0.40 and 0.45, however, the porosity and pore size of the PAFG samples increased, resulting in a decrease in compressive strength. The optimal L/F ratio was determined to be 0.35, which in line with the compressive strength results of the specimens.

Fig. 11 depicts SEM images of PAFG samples cured at various temperatures. Curing at 60 °C PAFG produced a denser geopolymer gel. This is due to the slower reaction kinetics when curing at 25 °C and the reduced degree of reaction due to water loss when curing at 90 °C. This provides evidence that the compressive strengths of the PAFG samples at 25 °C and 90 °C were slightly lower than those cured at 60 °C.

3.5. CO_2 emissions, energy consumption and economic analysis

The CO_2 emissions, energy consumption and cost of each raw materials are listed in Table 3. Alkali activators (NaOH and Na_2SiO_3) and cement are also listed for comparison with alkali-activated fly ash geopolymer (AAFG) and PC paste. Cement has a significantly greater CO_2 emissions, energy consumption, and cost than FA; consequently, FA-based geopolymers are regarded as a more sustainable material. Alkaline activators have higher CO_2 emissions and energy consumption than PA, but their cost is lower. This indicates that the use of PA may increase the cost of the geopolymer, so it is necessary to regulate the PA concentration.

In order to compare CO_2 emissions, energy consumption, and costs between various cementitious materials, AAFG and PC pastes with similar compressive strength to PAFG were chosen for the study. Typical mixture proportions of PAFG, AAFG and PC pastes, as well as their CO_2 emissions, energy consumption, and cost of 1 m^3 concrete are also summarized in Table 4. Due to the high CO_2 emissions and energy consumption of the alkaline activators, the mixture proportions of AAFG with activation of 4, 12 and 15 mol/L of NaOH solution were also collected. AAFG with activation of high concentration of NaOH are frequently correlated with increased CO_2 emissions, energy consumption, and costs. AAFG, which used Na_2SiO_3 as an activator, had greater CO_2 emissions, energy consumption, and costs. High-temperature curing of PAFG significantly increased CO_2 emissions, energy consumption, and costs, while limiting the increase in strength. Consequently, PAFG cured at room temperature has greater potential. Compared to AAFG activated by low concentration NaOH and PC pastes, the CO_2 emission

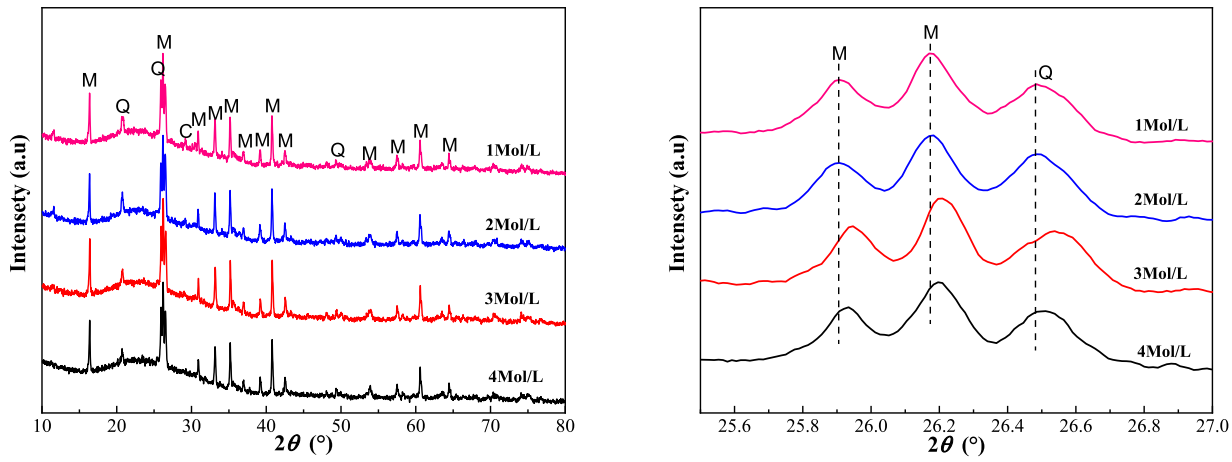

(a) PA concentration (L/F = 0.35, 60ºC)

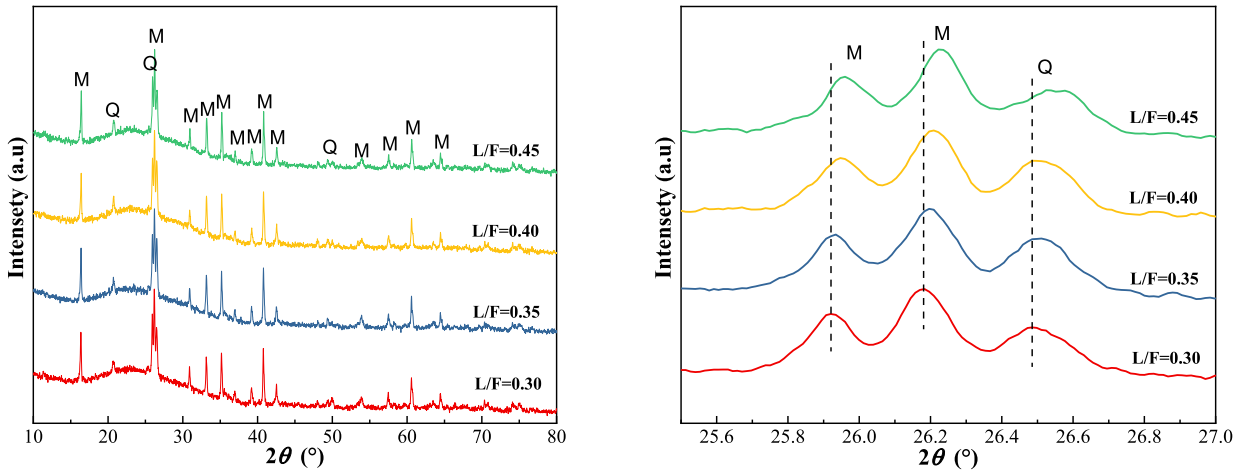

(b) L/F ratio (4 mol/L PA, 60ºC)

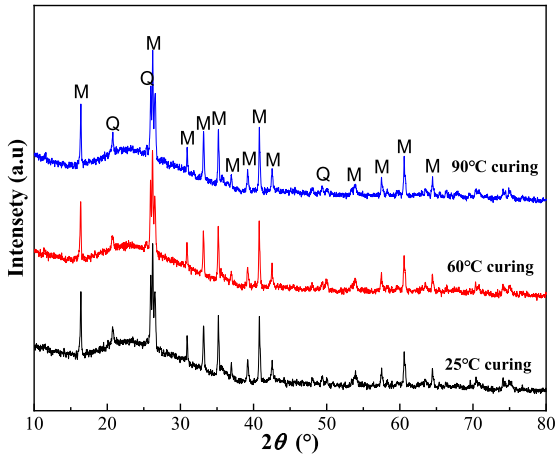

(c) Curing temperature (4 mol/L PA, L/F = 0.35)

Fig. 7. XRD patterns of PAFG (Q-Quarts, SiO_2; M-Mullite, $3Al_2O_3{\cdot}2SiO_2$; C-Calcite, $CaCO_3$).

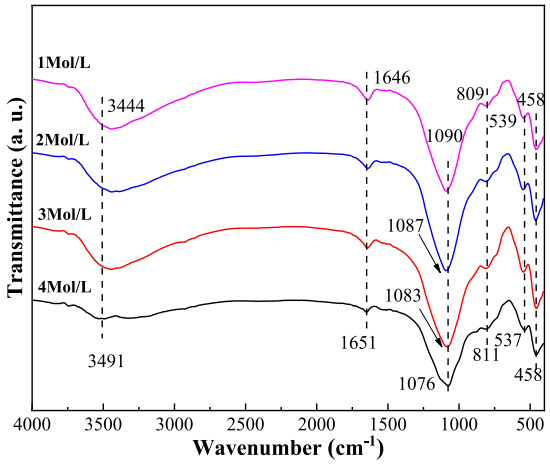

(a) PA concentration (L/F = 0.35, 60ºC)

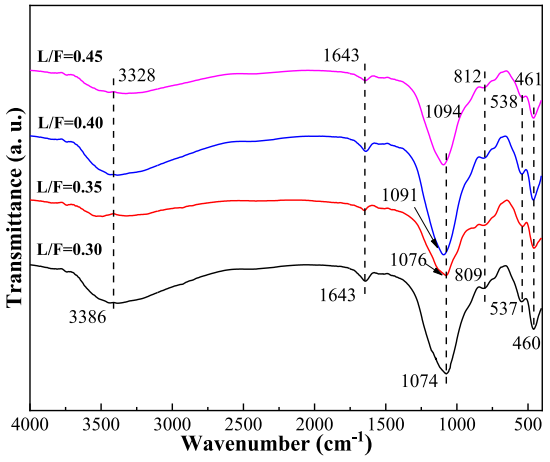

(b) L/F ratio (4 mol/L PA, 60ºC)

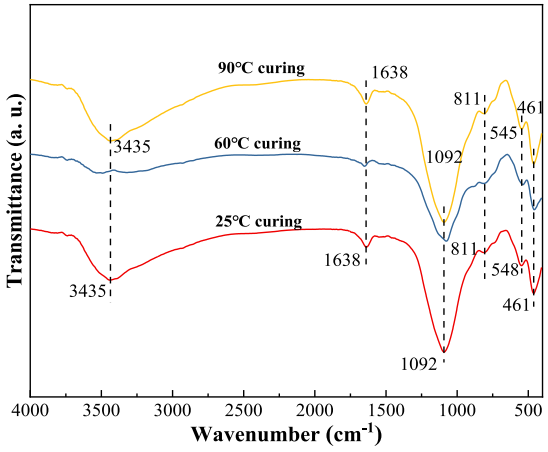

(c) Curing temperature (4 mol/L PA, L/F = 0.35)

Fig. 8. FTIR spectra of PAFG.

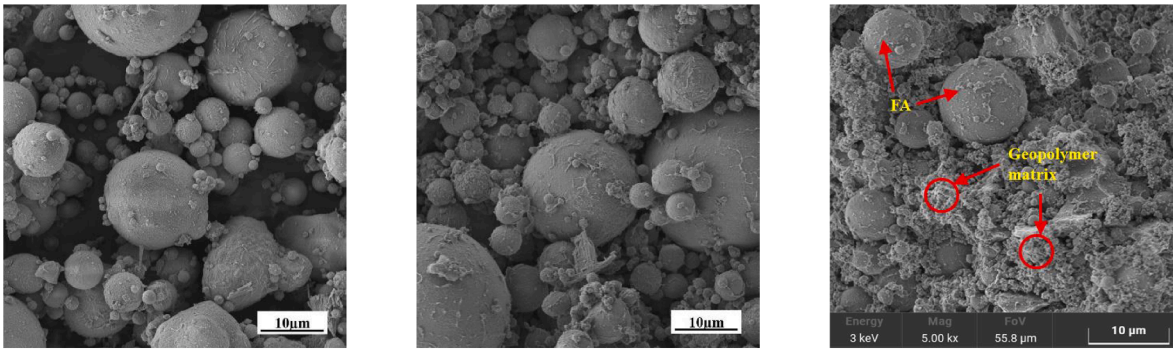

(a) 1 mol/L, 5000 × (b) 2 mol/L, 5000 × (c) 3 mol/L, 5000 ×

(d) 3 mol/L, 15000 × (e) 4 mol/L, 5000 × (f) 4 mol/L, 15000 ×

Fig. 9. SEM images of PAFG samples with L/F = 0.35 and 60 °C curing.

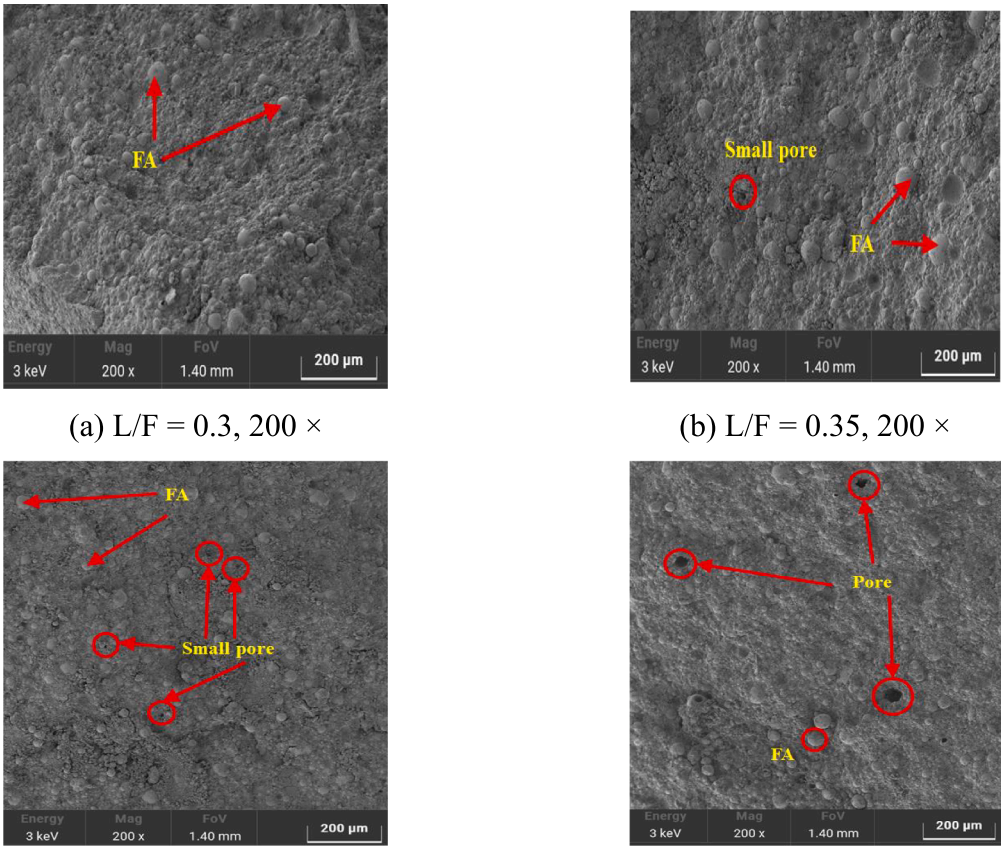

(a) L/F = 0.3, 200 × (b) L/F = 0.35, 200 ×

(c) L/F = 0.4, 200 × (d) L/F = 0.45, 200 ×

Fig. 10. SEM images of PAFG samples with 4 mol/L PA and 60 °C curing.

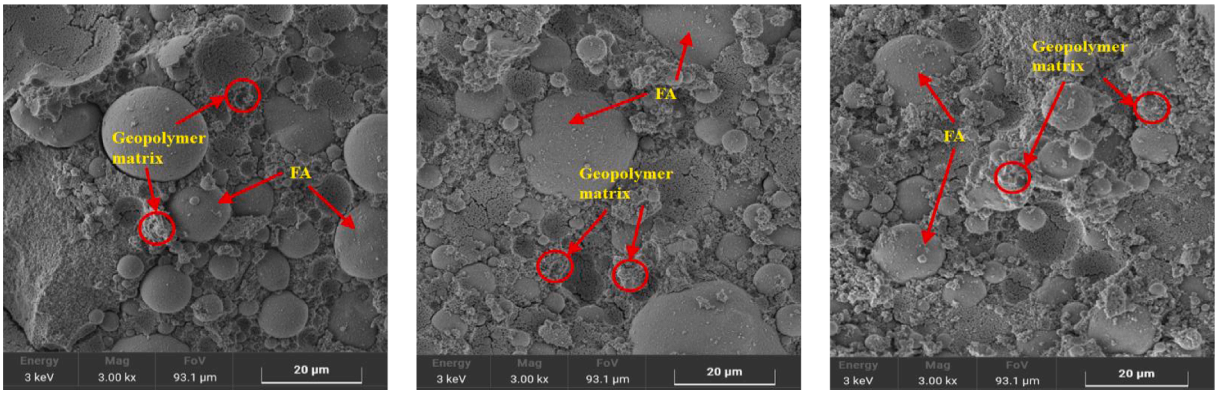

(a) 25°C, 3000 × (b) 60°C, 3000 × (c) 90°C, 3000 ×

Fig. 11. SEM images of PAFG samples with 4 mol/L PA and L/F = 0.35.

Table 3
CO_2 emissions, energy consumption and cost of each constituent of PC and geopolymers (transportation process is not considered).

Constituent	CO_2 emissions (kg/t)	Energy consumption (GJ/t)	Cost ($/t) [a]
FA [44]	12	0.173	45
Cement [45]	730	4.50	150
PA[b] [24,25]	314.4	1.17	812.76
NaOH [26]	1915	2.8	147.8
Na_2SiO_3[c] [26]	1222	5.371	264.44

[a] Market price may fluctuate;
[b] PA solution (85 wt%) was produced by the decomposition of phosphate rock with sulphuric acid;
[c] Sodium silicate liquids with weight ratio SiO_2/Na_2O of 2.4 and solid content of 40%, which are manufactured through melting of silica sand and sodium carbonate.

intensity and energy consumption intensity are decreased by 70.9% and 35.6%, and 90.6% and 90.6%, respectively. The costs increased by 87.4% and 30.7%, respectively, as a result of the high cost of PA solution. Therefore, it is essential to develop a mature and cost-effective PA preparation method for the production of PAFG.

4. Conclusions

In this study, the mechanical properties and microstructure of PAFG samples prepared with varying LPA concentrations, L/F ratios, and curing temperatures, as well as their effects on the environment and economy, were investigated. The following conclusions can be made from this study:

(1) The compressive strengths of PAFG with activation of LPA were generally low. The PAFG prepared with a L/F = 0.35 and 4 Mol PA solution curing at 60 °C for 6 days obtained the highest compressive strength of 13.23 MPa.
(2) The formation of geopolymer gels (Si-O-Al-O-P, Al-O-P, or Si-O-P) were the primary reaction products and strength gain for PAFG samples. The increase in PA concentration and L/F ratio accelerated the FA dealumination reaction and the polymerization reaction by increasing the H + and P-O concentrations of solution.
(3) SEM analysis revealed that increasing the concentration of PA, the L/F ratio, and the curing temperature facilitated the dissolution of FA particles and favored the polymerization reaction. However, an excessive L/F ratio increased porosity of specimens, which is detrimental to strength.

Table 4
Typical mixture proportions of PAFG, AAFG and PC pastes, as well as their CO_2 emissions, energy consumption, and cost.

Type	PAFG			AAFG				PC paste [46]
	P4L35 C25	P4L35 C60[a]	P4L35 C90[a]	NaOH-activated		$NaOH + Na_2SiO_3$-activated		
				[47]	[48]	[49]	[48]	
FA (kg/m^3)	1538.46	1538.46	1538.46	2127.66	1737.12	1195.22	1910.83	–
Cement (kg/m^3)	–	–	–	–	–	–	–	1333.33
PA[b] (kg/m^3)	172.09	172.09	172.09	–	–	–	–	–
NaOH (kg/m^3)	–	–	–	223.40 (12 mol/L)	98.53 (4 mol/L)	163.69 (15 mol/L)	43.35 (4 mol/L)	–
Na_2SiO_3[c] (kg/m^3)	–	–	–	–	–	336.25	183.44	–
Water[d] (kg/m^3)	366.37	366.37	366.37	414.89	596.32	735.12	537.54	800
Compressive strength (MPa)	11	13.23	11.39	17.3	8.18	10.5	7.35	12.3
Carbon emission (kg/m^3)	82.11	230.91	305.31	453.35	209.53	1355.06	666.36	973.33
Energy consumption (GJ/m^3)	0.50	1.37	1.80	1.00	0.58	5.18	2.91	6
Cost ($/m^3$)	233.78	255.38	266.18	128.76	92.73	300.27	213.67	200
Carbon intensity (kg/m^3/MPa)	7.46	17.45	26.81	26.21	25.61	129.05	90.66	79.13
Energy intensity (MJ/m^3/MPa)	45.74	103.34	157.96	57.69	70.97	493.03	396.00	487.8
Cost intensity ($/m^3$/MPa)	21.25	19.30	23.37	7.44	11.34	28.60	29.07	16.26

[a] At 60 °C and 90 °C, the power consumption at rated power is 240 and 360 kw·h for 6 days, respectively. CO_2 emissions, energy consumption, and costs for per kw·h of electricity are 0.62 kg, 3.6 MJ, and 0.09 $ respectively.
[b] PA referred to here is the solid content of the solution, excluding water.
[c] Sodium silicate referred to here is the solid content of the solution, excluding water.
[d] Water includes water in the activators and additional water.

(4) In comparison to low concentration NaOH-activated AAFG and PC pastes, the CO_2 emission intensity and energy consumption intensity of room temperature cured PAFG were reduced by 70.9% and 35.6%, and 90.6% and 90.6%, respectively. The cost increased by 87.4% and 30.7%, respectively, as a result of the higher price of PA solution. Therefore, it is essential to develop inexpensive chemical processes for the preparation of PA solutions.

CRediT authorship contribution statement

Min He: Conceptualization, Methodology, Data curation, Investigation, Writing – original draft. **Zongbao Yang:** Software, Writing – original draft. **Ning Li:** Conceptualization, Supervision, Writing – review & editing. **Xiaohong Zhu:** Writing – review & editing. **Bo Fu:** Methodology, Resources. **Zhihua Ou:** Supervision, Funding acquisition.

Declaration of Competing Interest

The authors declare that they have no known competing financial interests or personal relationships that could have appeared to influence the work reported in this paper.

Data availability

Data will be made available on request.

Acknowledgements

We gratefully acknowledge the support of the National Natural Science Foundation of China (51909086), Hunan Provincial Natural Science Foundation of China (2020JJ5131 and 2021JJ50044), Hunan Provincial Innovation Foundation for Postgraduate of China (CX20220831) and China Scholarship Council.

References

[1] L. Barcelo, J. Kline, G. Walenta, E. Gartner, Cement and carbon emissions, Mater. Struct. 47 (6) (2014) 1055–1065.
[2] N. Mahasenan, S. Smith, K. Humphreys, The Cement Industry and Global Climate Change: Current and Potential Future Cement Industry CO2 Emissions, in: J. Gale, Y. Kaya (Eds.), Greenhouse Gas Control Technologies – 6th International Conference, Pergamon, Oxford, 2003, pp. 995–1000.
[3] B.C. McLellan, R.P. Williams, J. Lay, A. van Riessen, G.D. Corder, Costs and carbon emissions for geopolymer pastes in comparison to ordinary Portland cement, J. Clean. Prod. 19 (9) (2011) 1080–1090.
[4] N. Li, C. Shi, Q. Wang, Z. Zhang, Z. Ou, Composition design and performance of alkali-activated cements, Mater. Struct. 50 (3) (2017) 178.
[5] Z. Liu, J. Wang, Q. Jiang, G. Cheng, L. Li, Y. Kang, D. Wang, A green route to sustainable alkali-activated materials by heat and chemical activation of lithium slag, J. Clean. Prod. 225 (2019) 1184–1193.
[6] C. Ng, U.J. Alengaram, L.S. Wong, K.H. Mo, M.Z. Jumaat, S. Ramesh, A review on microstructural study and compressive strength of geopolymer mortar, paste and concrete, Constr. Build. Mater. 186 (2018) 550–576.
[7] A. Nikolov, R. Titorenkova, N. Velinov, Z. Delcheva, Characterization of a novel geopolymer based on acid-activated fayalite slag from local copper industry.
[8] J. Davidovits, Geopolymer chemistry and applications, 2011: Institute Geopolymer, Saint Quentin, France, 2008.
[9] S. Pu, Z. Zhu, W. Song, W. Huo, J. Zhang, Mechanical and microscopic properties of fly ash phosphoric acid-based geopolymer paste: A comprehensive study, Constr. Build. Mater. 299 (2021) 123947.
[10] J.R. Njimou, M. Pengou, H.K. Tchakoute, M. Sieugaing Tamwa, C. Tizaoui, U. Fannang, P.N. Lemougna, C.P. Nanseu-Njiki, E. Ngameni, Removal of lead ions from aqueous solution using phosphate-based geopolymer cement composite, J. Chem. Technol. Biotechnol. 96 (5) (2021) 1358–1369.
[11] T. Dong, S. Xie, J. Wang, G. Zhao, Q. Song, Solidification and Stabilization of Spent TBP/OK Organic Liquids in a Phosphate Acid-Based Geopolymer, Sci. Technol. Nucl. Install. 2020 (2020) 8094205.
[12] S. Pu, Z. Zhu, W. Song, H. Wang, W. Huo, J. Zhang, A novel acidic phosphoric-based geopolymer binder for lead solidification/stabilization, J. Hazard. Mater. 415 (2021), 125659.
[13] Y.-S. Wang, J.-G. Dai, Z. Ding, W.-T. Xu, Phosphate-based geopolymer: Formation mechanism and thermal stability, Mater. Lett. 190 (2017) 209–212.
[14] Y.-S. Wang, Y. Alrefaei, J.-G. Dai, Silico-Aluminophosphate and Alkali-Aluminosilicate Geopolymers: A Comparative Review, Front. Mater. 6 (2019).
[15] M. Mahyar, S.T. Erdoğan, Phosphate-activated high-calcium fly ash acid-base cements, Cem. Concr. Compos. 63 (2015) 96–103.
[16] L. Le-ping, C. Xue-min, Q. Shu-heng, Y. Jun-li, Z. Lin, Preparation of phosphoric acid-based porous geopolymers, Appl. Clay Sci. 50 (4) (2010) 600–603.
[17] M. Zribi, S. Baklouti, Investigation of Phosphate based geopolymers formation mechanism, J. Non Cryst. Solids 562 (2021), 120777.
[18] K.-H. Yang, J.-K. Song, K.-I. Song, Assessment of CO2 reduction of alkali-activated concrete, J. Clean. Prod. 39 (2013) 265–272.
[19] A. Alsalman, L.N. Assi, R.S. Kareem, K. Carter, P. Ziehl, Energy and CO2 emission assessments of alkali-activated concrete and Ordinary Portland Cement concrete: A comparative analysis of different grades of concrete, Clean. Environ. Syst. 3 (2021), 100047.
[20] F. Pacheco-Torgal, Z. Abdollahnejad, S. Miraldo, M. Kheradmand, Alkali-activated cement-based binders (AACBs) as durable and cost-competitive low-CO2 binder materials: some shortcomings that need to be addressed, Handbook of low carbon concrete2017, pp. 195-216.
[21] A. Ababneh, F. Matalkah, R. Aqel, Synthesis of kaolin-based alkali-activated cement: carbon footprint, cost and energy assessment, J. Mater. Res. Technol. 9 (4) (2020) 8367–8378.
[22] P. Perez-Cortes, J.I. Escalante-Garcia, Alkali activated metakaolin with high limestone contents – Statistical modeling of strength and environmental and cost analyses, Cem. Concr. Compos. 106 (2020), 103450.
[23] S. Fernando, C. Gunasekara, D.W. Law, M.C.M. Nasvi, S. Setunge, R. Dissanayake, Life cycle assessment and cost analysis of fly ash–rice husk ash blended alkali-activated concrete, J. Environ. Manage. 295 (2021), 113140.
[24] R. Gilmour, Phosphoric Acid: Purification, Uses, Technology, and Economics, CRC Press, Boca Raton, 2013.
[25] National Greenhouse Accounts Factors, Australian Government Department of Industry, Science, Energy and Resources, Commonwealth of Australia, Canberra, 2020.
[26] L.K. Turner, F.G. Collins, Carbon dioxide equivalent (CO2-e) emissions: A comparison between geopolymer and OPC cement concrete, Constr. Build. Mater. 43 (2013) 125–130.
[27] T. Yang, X. Gao, J. Zhang, X. Zhuang, H. Wang, Z. Zhang, Sulphate resistance of one-part geopolymer synthesized by calcium carbide residue-sodium carbonate-activation of slag, Compos. B Eng. 242 (2022), 110024.
[28] X. Gao, X. Yao, T. Yang, S. Zhou, H. Wei, Z. Zhang, Calcium carbide residue as auxiliary activator for one-part sodium carbonate-activated slag cements: compressive strength, phase assemblage and environmental benefits, Constr. Build. Mater. 308 (2021), 125015.
[29] Y.-S. Wang, Y. Alrefaei, J.-G. Dai, Influence of coal fly ash on the early performance enhancement and formation mechanisms of silico-aluminophosphate geopolymer, Cem. Concr. Res. 127 (2020), 105932.
[30] Y.-S. Wang, J.L. Provis, J.-G. Dai, Role of soluble aluminum species in the activating solution for synthesis of silico-aluminophosphate geopolymers, Cem. Concr. Compos. 93 (2018) 186–195.
[31] ASTM C305, Standard practice for mechanical mixing of hydraulic cement pastes and mortars of plastic consistency, ASTM International, 2006.
[32] B.o. Fu, Z. Cheng, J. Han, N. Li, Understanding the Role of Metakaolin towards Mitigating the Shrinkage Behavior of Alkali-Activated Slag, Materials 14 (22) (2021) 6962.
[33] N. Li, C. Shi, Z. Zhang, D. Zhu, H.-J. Hwang, Y. Zhu, T. Sun, A mixture proportioning method for the development of performance-based alkali-activated slag-based concrete, Cem. Concr. Compos. 93 (2018) 163–174.
[34] N. Li, C. Shi, Z. Zhang, H. Wang, Y. Liu, A review on mixture design methods for geopolymer concrete, Compos. B Eng. 178 (2019), 107490.
[35] L. Gao, C. Xia, X. Hong, C. Wang, Effect of SiO2/Al2O3 molar ratio on microstructure and properties of phosphoric acid-based metakaolin geopolymerss, International Conference on Material Science and Civil Engineering, 2016.
[36] R. Li, G. Wu, L. Jiang, D. Sun, Interface microstructure and compressive behavior of fly ash/phosphate geopolymer hollow sphere structures, Mater. Des. (1980-2015) 65 (2015) 585-590.
[37] P. Scherrer, Estimation of the size and internal structure of colloidal particles by means of röntgen, Nachr. Ges. Wiss. Göttingen 2 (1918) 96–100.
[38] H. Douiri, S. Louati, S. Baklouti, M. Arous, Z. Fakhfakh, Structural, thermal and dielectric properties of phosphoric acid-based geopolymers with different amounts of H3PO4, Mater. Lett. 116 (2014) 9–12.
[39] S. Louati, S. Baklouti, B. Samet, Acid based geopolymerization kinetics: Effect of clay particle size, Appl. Clay Sci. 132–133 (2016) 571–578.
[40] K.Y. Wang, R.X. Liu, L. Zhang, Y.H. Yan, X.Y. Sui, C.L. Zhou, Z.Q. Cheng, Preparation and Thermal Stability of Quartz Fiber Reinforced Silicon Doped Aluminum Aerogel Composites, IOP Conf. Ser.: Mater. Sci. Eng. 678 (1) (2019), 012076.
[41] Y. Cai, J. Xue, D.A. Polya, A Fourier transform infrared spectroscopic study of Mg-rich, Mg-poor and acid leached palygorskites, Spectrochim. Acta A Mol. Biomol. Spectrosc. 66 (2) (2007) 282–288.
[42] A. Fernández-Jiménez, A. Palomo, Composition and microstructure of alkali activated fly ash binder: Effect of the activator, Cem. Concr. Res. 35 (10) (2005) 1984–1992.
[43] N. Li, N. Farzadnia, C. Shi, Microstructural changes in alkali-activated slag mortars induced by accelerated carbonation, Cem. Concr. Res. 100 (2017) 214–226.
[44] G.F. Huseien, A.R.M. Sam, K.W. Shah, J. Mirza, M.M. Tahir, Evaluation of alkali-activated mortars containing high volume waste ceramic powder and fly ash replacing GBFS, Constr. Build. Mater. 210 (2019) 78–92.

[45] I. Faridmehr, M.L. Nehdi, M. Nikoo, G.F. Huseien, T. Ozbakkaloglu, Life-Cycle Assessment of Alkali-Activated Materials Incorporating Industrial Byproducts, Materials 14 (9) (2021) 2401.
[46] B. Fang, T. Xu, S. Shuang, Laboratory Study on Cement Slurry Formulation and Its Strength Mechanism for Semi-Flexible Pavement, J. Test. Eval. 44 (2016) 907–913.
[47] A. Palomo, M.W. Grutzeck, M.T. Blanco, Alkali-activated fly ashes: A cement for the future, Cem. Concr. Res. 29 (8) (1999) 1323–1329.
[48] S. Sasui, G. Kim, J. Nam, T. Koyama, S. Chansomsak, Strength and Microstructure of Class-C Fly Ash and GGBS Blend Geopolymer Activated in NaOH & NaOH + Na2SiO3, Materials, 2020.
[49] P. Chindaprasirt, P. Paisitsrisawat, U. Rattanasak, Strength and resistance to sulfate and sulfuric acid of ground fluidized bed combustion fly ash–silica fume alkali-activated composite, Adv. Powder Technol. 25 (3) (2014) 1087–1093.